AIP Applied Physics Letters

High-power low-droop violet semipolar $(30\bar{3}\bar{1})$ InGaN/GaN light-emitting diodes with thick active layer design

Daniel L. Becerra, Yuji Zhao, Sang Ho Oh, Christopher D. Pynn, Kenji Fujito, Steven P. DenBaars, and Shuji Nakamura

Citation: Applied Physics Letters **105**, 171106 (2014); doi: 10.1063/1.4900793
View online: http://dx.doi.org/10.1063/1.4900793
View Table of Contents: http://scitation.aip.org/content/aip/journal/apl/105/17?ver=pdfcov
Published by the AIP Publishing

Articles you may be interested in
p-doping-free InGaN/GaN light-emitting diode driven by three-dimensional hole gas
Appl. Phys. Lett. **103**, 263501 (2013); 10.1063/1.4858386

Three-dimensional GaN templates for molecular beam epitaxy of nonpolar InGaN/GaN coaxial light-emitting diodes
J. Vac. Sci. Technol. B **31**, 03C107 (2013); 10.1116/1.4792519

Efficiency and droop improvement in green InGaN/GaN light-emitting diodes on GaN nanorods template with SiO2 nanomasks
Appl. Phys. Lett. **101**, 233104 (2012); 10.1063/1.4768950

Efficiency droop alleviation in InGaN/GaN light-emitting diodes by graded-thickness multiple quantum wells
Appl. Phys. Lett. **97**, 181101 (2010); 10.1063/1.3507891

High-power and reliable operation of vertical light-emitting diodes on bulk GaN
Appl. Phys. Lett. **85**, 3971 (2004); 10.1063/1.1810631

This article is copyrighted as indicated in the article. Reuse of AIP content is subject to the terms at: http://scitation.aip.org/termsconditions. Downloaded to IP: 149.169.207.65 On: Fri, 31 Oct 2014 16:33:26

APPLIED PHYSICS LETTERS **105**, 171106 (2014)

CrossMark

High-power low-droop violet semipolar $(30\bar{3}\bar{1})$ InGaN/GaN light-emitting diodes with thick active layer design

Daniel L. Becerra,[1,a)] Yuji Zhao,[1] Sang Ho Oh,[2] Christopher D. Pynn,[1] Kenji Fujito,[3] Steven P. DenBaars,[1,2] and Shuji Nakamura[1,2]

[1]*Materials Department, University of California, Santa Barbara, California 93106, USA*
[2]*Department of Electrical and Computer Engineering, University of California, Santa Barbara, California 93106, USA*
[3]*Optoelectronic Laboratory, Mitsubishi Chemical Corporation, 1000 Higashi-Mamiana, Ushiku, Ibaraki 300-1295, Japan*

(Received 2 October 2014; accepted 19 October 2014; published online 29 October 2014)

Devices grown on nonpolar and semipolar planes of GaN offer key performance advantages over devices grown on the conventional *c*-plane, including reduced polarization fields. This allows for a wider design space on semipolar planes for light emitting diodes (LEDs) to address the problem of efficiency droop at high current densities. LED structures with very thick (10–100 nm) InGaN single-quantum-well/double heterostructure active regions were grown using conventional metal organic chemical vapor deposition on semipolar $(30\bar{3}\bar{1})$ free-standing GaN substrates and processed and packaged using conventional techniques. Simulated band diagrams showed reduced polarization fields on the $(30\bar{3}\bar{1})$ plane. The calculated critical thickness for misfit dislocation formation is higher on the $(30\bar{3}\bar{1})$ plane than on other semipolar planes, such as $(20\bar{2}\bar{1})$, allowing for thicker active regions than our previous work to further reduce droop. The higher critical thickness was confirmed with defect characterization via cathodoluminescence. A trend is demonstrated in lower efficiency droop for devices with thicker active regions. Thermal droop characteristics of these devices are also presented. These observed results were utilized to demonstrate over 1 W of output power at a current density of 1 kA/cm^2 from a single 0.1 mm^2 LED device. © *2014 AIP Publishing LLC*. [http://dx.doi.org/10.1063/1.4900793]

The efficiency of conventional (Al, Ga, In)N-based light-emitting diodes (LEDs) grown on the polar *c*-plane drops dramatically at high current densities. This problem, known as efficiency droop, presents significant challenges to the fabrication of high power and high efficiency devices.[1–3] The droop effect is further exacerbated for the thin (2–3 nm) quantum wells (QWs) used in conventional *c*-plane devices—a device structure used to compensate the low electron-hole wavefunction overlap and quantum confined Stark effect (QCSE).[4,5] This leads to an increased current density in the active region and a further increased droop effect on *c*-plane devices. More complex structures such as InGaN/GaN multiple-quantum-wells (MQWs) were utilized to enhance the efficiency and reduce the droop on *c*-plane devices.[4,5] However, the results are less than satisfactory due to the issues such as carrier transport, non-uniform carrier distributions in the wells, and still present polarization-related effects. Additionally, the phenomenon of thermal droop, where the external quantum efficiency (EQE) of devices decreases with increasing temperature, while less studied than current droop, is also an issue for nitride LEDs.[6,7]

Alternatively, growth on nonpolar or semipolar planes of GaN holds great promise for high performance devices, due to the reduction of the polarization fields and the QCSE. Certain semipolar devices have already shown improved performance with reduced efficiency droop. For example, LEDs grown on the semipolar $(20\bar{2}\bar{1})$ plane have been demonstrated with low efficiency droop up to 400 A/cm^2.[8,9] It was argued that the low polarization-related electric fields and high-quality InGaN layer allows for LED structures with a relatively thick active layer which are favorable for reducing efficiency droop.[9] The carrier density dependent Auger recombination effect, recently shown to be a primary contributor to droop[10] should be reduced for these thicker active layers. Additional advantages including high optical polarization ratio, high indium incorporation, small wavelength shift, and narrow spectral linewidth were also reported for semipolar $(20\bar{2}\bar{1})$ LEDs and lasers.[11–13] However, more radical device structures and material advances are required to further improve the device performance.

In this paper, we report high power and low droop violet InGaN LEDs fabricated on the semipolar $(30\bar{3}\bar{1})$ plane, which is a semipolar plane with high inclination angle (~80°) with respect to *c*-plane. The low polarization-related effects and large critical thickness on the $(30\bar{3}\bar{1})$ plane enabled radical LED structures with very thick InGaN active layers, including single-quantum-wells (SQWs) and double heterostructures (DHs) with thickness ranging from 10 to 100 nm. Experimental results for both current droop and thermal droop are presented for LEDs with different active layer thicknesses. We also report a high-performance low-droop small-area (0.1 mm^2) semipolar $(30\bar{3}\bar{1})$ LED with over 1 W of light-output-power (LOP) at current density of 1 kA/cm^2, using this thick active layer design.

LED structures were grown by conventional metal organic chemical vapor deposition (MOCVD) on free-standing $(30\bar{3}\bar{1})$ GaN substrates supplied by Mitsubishi Chemical Corporation. The device structure consisted of a

[a)]Email: dbecerra@engineering.ucsb.edu

 © 2014 AIP Publishing LLC

This article is copyrighted as indicated in the article. Reuse of AIP content is subject to the terms at: http://scitation.aip.org/termsconditions. Downloaded to IP: 149.169.207.65 On: Fri, 31 Oct 2014 16:33:26

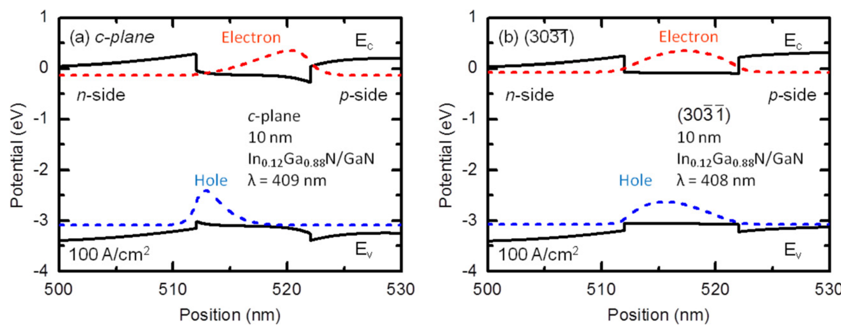

FIG. 1. Simulated band diagrams for 10 nm thick violet SQW at 100 A/cm^2 on (a) *c*-plane GaN and (b) $(30\bar{3}\bar{1})$ GaN.

1 μm Si-doped *n*-type GaN layer, a ten-period Si-doped InGaN/GaN 3 nm/3 nm superlattice, a 15 nm thick lower GaN barrier, an InGaN active region with various layer thickness ranging from 10 nm to 100 nm, a 10 nm thick upper GaN barrier, a 16 nm Mg-doped $Al_{0.15}Ga_{0.85}N$ electron blocking layer (EBL), and a 60 nm *p*-type GaN layer.

Figure 1 demonstrates the calculated band diagram profiles for violet *c*-plane and $(30\bar{3}\bar{1})$ LEDs with a 10 nm thick $In_{0.12}Ga_{0.9}N$ active layer at a current density of 100 A/cm^2, using the commercial SiLENSe package developed by the STR Group. The potential distributions were calculated by solving the Schrödinger-Poisson equations self-consistently and include strain and polarization effects. The details for the methods used to calculate the band diagrams can be found in Ref. 12. For *c*-plane InGaN/GaN devices, it is well understood that due to the large polarization-related electric fields, the electrons and holes in the active region will be pushed apart in opposite directions, which results in a distorted energy band diagram profile, a low electron-hole wavefunction overlap, and subsequently a low radiative recombination efficiency. For semipolar $(30\bar{3}\bar{1})$ devices, on the other hand, the polarization-related electric fields are much smaller than the *c*-plane case and a flat band diagram profile with high electron-hole wavefunction overlap can be obtained. It is noteworthy that this low wavefunction overlap problem will become more prominent for *c*-plane structures with increased active layer thickness, while the semipolar $(30\bar{3}\bar{1})$ structures can maintain a high wavefunction overlap (>0.9) with very thick active layers.

Figure 2 presents the Matthews–Blakeslee equilibrium critical thickness values (calculated under the assumption of isotropic elasticity) for InGaN/GaN structures on various semipolar planes.[14] Growth of thick strained heterostructures on nonpolar and semipolar planes often leads to the formation of misfit dislocations (MDs) at heterointerfaces via dislocation glide on the available slip planes.[15] The driving force for such dislocation glide originates from the resolved shear stress on the slip plane. Since the preferred slip plane in wurtzite GaN is the basal *c*-plane, we refer to this as basal plane (BP) slip. The resolved stress first increases with inclination angle from c plane to a maximum at about 45°, then decreases with increasing inclination angle from the *c*-plane. Therefore, semipolar planes with high inclination angles (with respect to *c*-plane) such as the $(30\bar{3}\bar{1})$ plane will have an increased critical thickness for strained InGaN layers compared to other planes (Fig. 2), due to the reduction in the resolved shear stress on the basal plane. Relaxation has been observed both above and below this calculated thickness.[16,17] Kinetic factors such as Peierls barriers and/or existing threading dislocation geometries are suggested to be possible causes of this.[17] Additionally, relaxation along other planes besides the basal *c*-plane has been observed.[18] The activation of these other slip systems, which we refer to as 2D relaxation or non-basal plane (NBP) slip, can depend on those same kinetic factors that cause the deviation from the calculated basal plane relaxation critical thickness, and are also plane dependent.[17] The misfit dislocations caused by these non-basal plane slip systems can have a more dramatic effect on device performance, as shown below.

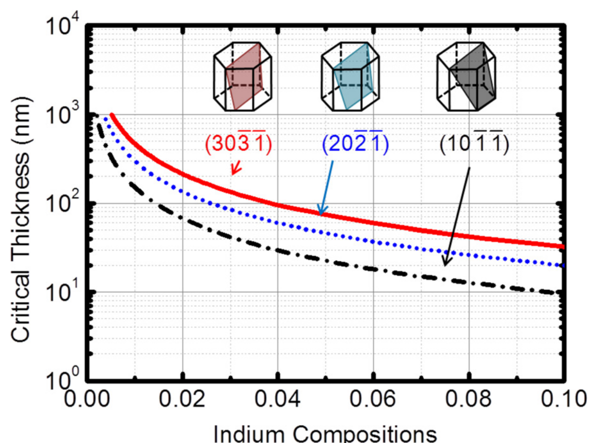

FIG. 2. Calculated Matthews-Blakeslee critical thickness for various semipolar planes of GaN.

Figure 3(a) shows the electroluminescence light-output power as a function of active layer thickness for full LED structures grown on the $(20\bar{2}\bar{1})$ and $(30\bar{3}\bar{1})$ planes. At low active layer thickness, the $(20\bar{2}\bar{1})$ LEDs showed comparable performance with $(30\bar{3}\bar{1})$ devices. When the InGaN layer exceeds its critical thickness (~20 nm), however, the $(20\bar{2}\bar{1})$ device performance drops dramatically. In contrast, the $(30\bar{3}\bar{1})$ LEDs showed higher performance with thicker active layer structures than the $(20\bar{2}\bar{1})$ devices due to the higher critical thickness. The optical performance of the devices was further illuminated by material characterization. Figures 3(b)–3(g) show representative panchromatic cathodoluminescence (CL) images demonstrating the progression of defect generation and stress relaxation in $(20\bar{2}\bar{1})$ and $(30\bar{3}\bar{1})$ devices. At 20 nm, a few dark lines parallel to the *a*-direction (BP MDs) are visible for the $(20\bar{2}\bar{1})$ devices. We can also see the presence of very small NBP MDs, indicating the onset of performance-degrading 2D relaxation. Starting from 40 nm, a significant amount of non-basal plane dark defects are seen on $(20\bar{2}\bar{1})$ devices, indicating that the InGaN layers were experiencing stronger 2D relaxation as the thickness

This article is copyrighted as indicated in the article. Reuse of AIP content is subject to the terms at: http://scitation.aip.org/termsconditions. Downloaded to IP: 149.169.207.65 On: Fri, 31 Oct 2014 16:33:26

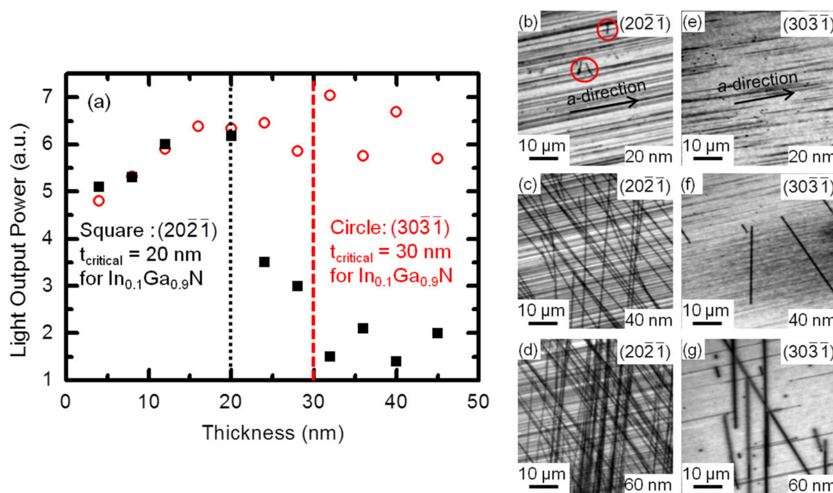

FIG. 3. (a) Electroluminescence light output power versus thickness of QW/DH comparing $(20\bar{2}\bar{1})$ and $(30\bar{3}\bar{1})$. The MB critical thickness is overlaid. (b)–(d) panchromatic CL images of $(20\bar{2}\bar{1})$ LED structures for 20, 40, and 60 nm thick active regions, respectively. The circles in (b) highlight small NBP misfit dislocations. (e)–(g) panchromatic CL images of $(30\bar{3}\bar{1})$ LED structures for 20, 40, and 60 nm thick active regions, respectively.

increased, corresponding to the low output power. The $(30\bar{3}\bar{1})$ structures showed similar trends with $(20\bar{2}\bar{1})$ devices. However, due to the increased critical thickness, we see no NBP MDs on the 20 nm images, and significantly fewer NBP MDs for 40 nm and 60 nm cases. This indicates that the $(30\bar{3}\bar{1})$ samples were less relaxed compared to $(20\bar{2}\bar{1})$ devices, and it also indicates that BP misfit dislocations do not have a large impact on device performance, especially for thick InGaN layers. This is consistent with the device results in Fig. 3(a). A thorough material study including x-ray diffraction analysis (XRD) and transmission electron microscopy (TEM) is currently underway and will be published elsewhere.

For the LED device fabrication, a rectangular mesa pattern (active area of 0.1 mm^2) was formed by conventional lithography and chlorine-based inductively coupled plasma (ICP) etching after an indium tin oxide (ITO) current spreading layer was deposited by electron beam evaporation. Ti/Al/Ni/Au n-type contacts and Cr/Ni/Au *p*- and n-pads were deposited by electron beam evaporation and a conventional lift-off process. The back side of the devices was roughened using a procedure published elsewhere.[19] The devices were then diced and mounted on a silver header and encapsulated in silicone.

Figure 4(a) presents the EQE as a function of current density for $(30\bar{3}\bar{1})$ LEDs with various active layer thicknesses under pulsed operation (1% duty cycle). The LEDs with the lowest InGaN thickness (10 nm) showed the highest peak efficiency. We see the peak efficiency decreases with increasing active region thickness, and is also shifted to higher current densities. Figure 4(b) shows the same data plotted with normalized EQE versus current density on a logarithmic scale. The data in this figure show a trend with lower EQE droop with increasing active region thickness.

Figure 5 shows EQE versus current density at different device temperatures. A decrease can be seen in EQE as the temperature increases as has been identified elsewhere.[7] This is termed as thermal droop. In order to quantify the thermal droop, a factor known as the hot/cold (H/C) factor is used. This is defined as: hot/cold factor = $EQE_{100\,^{\circ}C}/EQE_{20\,^{\circ}C}$. The devices with relatively thin active regions (10–40 nm) showed improved thermal characteristics with only 10% EQE droop at 120 °C, corresponding to a H/C factor of 0.9, similar to that of devices with thick active regions on the $(20\bar{2}\bar{1})$ plane.[7] Figure 5(a) shows a representative curve for the 20 nm thick active region device. As the active regions became thicker, the thermal performance suffers. Figure 5(b) shows the performance of the 100 nm thick active region device, which showed 20% EQE droop at 120 °C (H/C factor of 0.8).

The above studies were used to optimize a device structure to obtain the highest performance. An active layer thickness of 15 nm was selected and a device was fabricated as discussed above, but packaged using a vertical transparent packaging method.[20] Figure 6(a) shows the EQE and LOP of the small-area 0.1 mm^2 LED device under pulsed operation (1% duty cycle). We see a peak EQE above 50% drooping to only 33% at a current density of 1 kA/cm^2 and power of 1008.7 mW at 1 kA/cm^2. Figure 6(b) shows the wavelength and full width at half maximum (FWHM) of the emission spectrum. We see a very small wavelength shift of only a few nm up to 1 kA/cm^2 and a low FWHM.

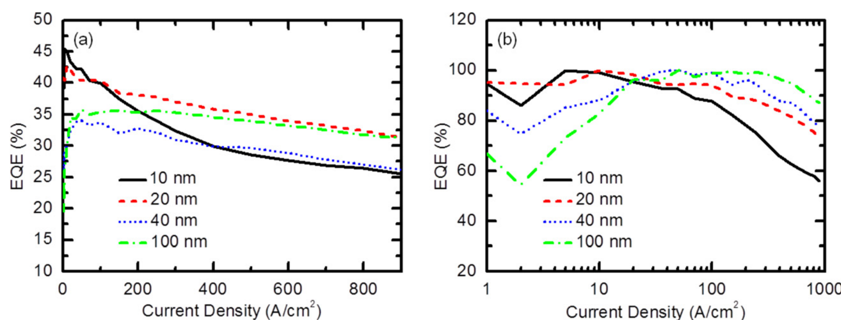

FIG. 4. (a) Absolute EQE versus current density and (b) normalized EQE versus current density on a logarithmic scale for LED devices with active region thickness 10–100 nm (pulsed condition, 1% duty cycle).

This article is copyrighted as indicated in the article. Reuse of AIP content is subject to the terms at: http://scitation.aip.org/termsconditions. Downloaded to IP: 149.169.207.65 On: Fri, 31 Oct 2014 16:33:26

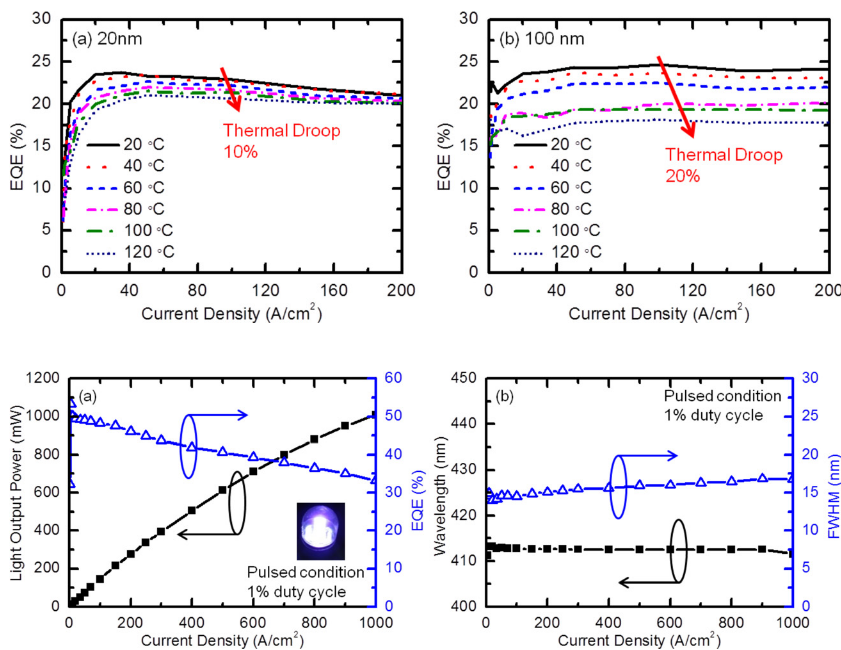

FIG. 5. EQE versus current density measured at different temperatures for devices with a (a) 20 nm thick active region and (b) 100 nm thick active region.

FIG. 6. (a) Output power and EQE versus current density for a packaged LED device with a 15 nm thick SQW active region (pulsed condition, 1% duty cycle). (b) Peak wavelength and FWHM for the device as a function of current density.

In summary, LED devices with very thick active regions of 10–100 nm were grown on the $(30\bar{3}\bar{1})$ plane of GaN. Utilizing the low polarization fields and high critical thickness of this plane, high power low droop LEDs were fabricated. Electroluminescence and cathodoluminescence confirmed fewer 2D dislocations on $(30\bar{3}\bar{1})$ devices led to higher performance at very thick active regions. A trend in lower droop with thicker active region thickness was demonstrated. The results of this study led to the fabrication of a small-area 0.1 mm^2 LED with over 1 W of output power at 1 kA/cm^2.

The authors thank Erin C. Young for helpful discussions on relaxation. The authors acknowledge the support of the Solid State Lighting and Energy Center/Solid State Lighting and Energy Electronics Center (SSLEC/SSLEEC) at UCSB. A portion of this work was done in the UCSB nanofabrication facility, part of the National Science Foundation funded NNIN. This work made use of MRL Central Facilities supported by the MRSEC Program of the National Science Foundation under Award No. DMR05-20415.

[1]S. Nakamura and M. R. Krames, Proc. IEEE **101**, 2211 (2013).
[2]Y. C. Shen, G. O. Mueller, S. Watanabe, N. F. Gardner, A. Munkholm, and M. R. Krames, Appl. Phys. Lett. **91**, 141101 (2007).
[3]E. Kioupakis, P. Rinke, K. T. Delaney, and C. G. Van de Walle, Appl. Phys. Lett. **98**, 161107 (2011).
[4]F. Bernardini, V. Fiorentini, and D. Vanderbilt, Phys. Rev. B **56**, R10024 (1997).
[5]V. Fiorentini, F. Bernardini, F. Della Sala, A. Di Carlo, and P. Lugli, Phys. Rev. B **60**, 8849 (1999).
[6]D. S. Meyaard, Q. Shan, J. Cho, E. Fred Schubert, S.-H. Han, M.-H. Kim, C. Sone, S. Jae Oh, and J. Kyu Kim, Appl. Phys. Lett. **100**, 081106 (2012).
[7]C. C. Pan, T. Gilbert, N. Pfaff, S. Tanaka, Y. Zhao, D. Feezell, J. S. Speck, S. Nakamura, and S. P. DenBaars, Appl. Phys. Express **5**, 102103 (2012).
[8]Y. Zhao, S. Tanaka, C.-C. Pan, K. Fujito, D. Feezell, J. S. Speck, S. P. DenBaars, and S. Nakamura, Appl. Phys. Express **4**, 082104 (2011).
[9]C. C. Pan, S. Tanaka, F. Wu, Y. Zhao, J. S. Speck, S. Nakamura, S. P. DenBaars, and D. Feezell, Appl. Phys. Express **5**, 062103 (2012).
[10]J. Iveland, L. Martinelli, J. Peretti, J. S. Speck, and C. Weisbuch, Phys. Rev. Lett. **110**, 177406 (2013).
[11]Y. Zhao, S. Tanaka, Q. Yan, C. Y. Huang, R. B. Chung, C. C. Pan, K. Fujito, D. Feezell, C. G. Van de Walle, J. S. Speck, S. P. DenBaars, and S. Nakamura, Appl. Phys. Lett. **99**, 051109 (2011).
[12]Y. Zhao, Q. Yan, C. Y. Huang, S. C. Huang, P. S. Hsu, S. Tanaka, C. C. Pan, Y. Kawaguchi, K. Fujito, C. G. Van de Walle, J. S. Speck, S. P. DenBaars, S. Nakamura, and D. Feezell, Appl. Phys. Lett. **100**, 201108 (2012).
[13]Y. Zhao, S. H. Oh, F. Wu, Y. Kawaguchi, S. Tanaka, K. Fujito, J. S. Speck, S. P. DenBaars, and S. Nakamura, Appl. Phys. Express **6**, 062102 (2013).
[14]J. W. Matthews and A. E. Blakeslee, J. Cryst. Growth **27**, 118 (1974).
[15]A. E. Romanov, E. C. Young, F. Wu, A. Tyagi, C. S. Gallinat, S. Nakamura, S. P. DenBaars, and J. S. Speck, J. Appl. Phys. **109**, 103522 (2011).
[16]I. L. Koslow, M. T. Hardy, P. Shan Hsu, F. Wu, A. E. Romanov, E. C. Young, S. Nakamura, S. P. DenBaars, and J. S. Speck, J. Cryst. Growth **388**, 48 (2014).
[17]P. S. Hsu, M. T. Hardy, E. C. Young, A. E. Romanov, S. P. DenBaars, S. Nakamura, and J. S. Speck, Appl. Phys. Lett. **100**, 171917 (2012).
[18]M. T. Hardy, P. S. Hsu, F. Wu, I. L. Koslow, E. C. Young, S. Nakamura, A. E. Romanov, S. P. Denbaars, and J. S. Speck, Appl. Phys. Lett. **100**, 202103 (2012).
[19]Y. Zhao, J. Sonoda, C.-C. Pan, S. Brinkley, I. Koslow, K. Fujito, H. Ohta, S. P. DenBaars, and S. Nakamura, Appl. Phys. Express **3**, 102101 (2010).
[20]C. C. Pan, I. Koslow, J. Sonoda, H. Ohta, J. S. Ha, S. Nakamura, and S. P. Denbaars, Jpn. J. Appl. Phys., Part 1 **49**, 080210 (2010).

This article is copyrighted as indicated in the article. Reuse of AIP content is subject to the terms at: http://scitation.aip.org/termsconditions. Downloaded to IP: 149.169.207.65 On: Fri, 31 Oct 2014 16:33:26